Journal Pre-proofs

Zn-Fe Flower-like Nanoparticles Growth by Gas Condensation

H. Lamsaf, V. Lenzi, L. Marques, L. Rebouta, S. Carvalho, L.F. Ballesteros, M.A. Cerqueira, J.A. Teixeira, L. Pastrana, S. Calderon V

PII: S0167-577X(21)00612-1
DOI: https://doi.org/10.1016/j.matlet.2021.129916
Reference: MLBLUE 129916

To appear in: *Materials Letters*

Received Date: 1 March 2021
Revised Date: 15 April 2021
Accepted Date: 16 April 2021

Please cite this article as: H. Lamsaf, V. Lenzi, L. Marques, L. Rebouta, S. Carvalho, L.F. Ballesteros, M.A. Cerqueira, J.A. Teixeira, L. Pastrana, S. Calderon V, Zn-Fe Flower-like Nanoparticles Growth by Gas Condensation, *Materials Letters* (2021), doi: https://doi.org/10.1016/j.matlet.2021.129916

Zn-Fe Flower-like Nanoparticles Growth by Gas Condensation

H. Lamsaf [1,2], V. Lenzi [1], L. Marques [1], L. Rebouta [1], S. Carvalho [4], L. F. Ballesteros [1,3], M. A. Cerqueira [2], J. A. Teixeira [3], L. Pastrana [2], S. Calderon V [1,2] *.

[1] CF-UM-UP, Centre of Physics of Minho and Porto Universities, Campus of Azurém, 4800-058 Guimarães, Portugal
[2] INL - International Iberian Nanotechnology Laboratory, Av. Mestre José Veiga s/n, 4715-330 Braga, Portugal
[3] CEB – Centre of Biological Engineering, University of Minho, Campus of Gualtar, 4710-057 Braga, Portugal
[4] SEG-CEMMPRE, Mechanical Engineering Department, University of Coimbra, 3030-788 Coimbra, Portugal

*** Corresponding author: secave44@gmail.com**

Abstract

Bimetallic nanoparticles have gained attention in the last decade due to their unusual characteristics compared to monometallic counterparts. However, production of such particles with controlled morphologies and composition need to be explored and the mechanisms understood. In this work, we demonstrate a fast and simple process to obtain flower-like Zn-Fe (Zinc-Iron) nanoparticles (NPs) using a hybrid system based on the combination of conventional magnetron sputtering and a cluster beam source. The morphology and structure were characterized by Scanning transmission electron microscopy (STEM), while the chemical composition was evaluated by simultaneous acquisition of Energy-dispersive X-ray spectroscopy (EDS) and Electron energy loss spectroscopy (EELS). Besides, molecular dynamic simulations were used to model the nanoparticle collisions during the simultaneous production, revealing the formation mechanisms of the flower-like nanoparticles.

Keywords: bimetallic; STEM; EELS tomography; oxygen scavengers; nanomaterial.

Introduction

Hybrid metallic nanoparticles (NPs) have shown enormous potential in a variety of fields, including materials for biomedical, catalysis, sensors, energy [1-2] , and food packaging applications [3]. These heterostructures are characterized by a synergetic effect among the components, which provides not only the functionalities of each metal but also enhanced properties due to additional features provided by the interface of their components. Their chemical composition, morphology, and concentration define the functional characteristics. However, to properly control the morphology and composition of the NPs, the growth mechanisms of these heterostructures must be well understood. This kind of nanostructures are usually produced by physical, chemical, and biological methods [4]. However, magnetron sputtering is one of the techniques that allow a control of the distribution, size,

and composition, besides the non-toxicity of the samples thanks to the absence of chemical solvents [5].

We have previously reported the production of individual Zn particles supported by a carbon substrate using classical magnetron sputtering[5], and the production of metallic particles using cluster beam sources coupled to a vacuum chamber has also been reported [6-7]. Their morphology can be controlled by the deposition conditions, varying from spherical to cubic NPs. Besides, the formation of core-shell and Janus-like particles is also well-known. However, these multi-element NPs are usually produced using a complex cluster beam source setup, where more than one magnetron allows the condensation of the particles inside the cluster gun chamber.

To simplify this process, we designed a simple and fast production methodology of flower-like Zn-Fe NPs and explored the growth mechanisms taking place during the production.

Experimental details

Zn-Fe NPs were produced using a magnetron sputtering chamber equipped with a cluster gun. The process consisted in applying, during 1 min, a density current of 2.96 $mA.cm^{-2}$ and 2.67 $mA.cm^{-2}$ to Zn (principal chamber) and Fe (cluster gun) targets, under an Argon working pressure of 0.8 Pa and 70 Pa, respectively.

The materials were characterized using high-angle annular dark-field (HAADF) STEM images, Energy-dispersive X-ray spectroscopy mappings (EDS-mapping) and Electron Energy Loss Spectroscopy (EELS) acquired on a double corrected FEI Titan Themis operated at 200keV.

Finally, molecular dynamic simulations were carried out to elucidate the growth mechanism of the particles, using LAMMPS [8]. Cu NPs were chosen for the MD simulations in lieu of Zn NPs because of similar atomic masses and the lack of a suitable MD force-field for the iron-zinc pair.

More detailed information can be found in supplementary information (Figure S1-S3).

Results and discussion

Fe or Zn NPs oxidize spontaneously when contacting oxygen in the environment, forming a passivation layer that prevents further oxidation. Thus, when they are produced separately, core-shell nanostructures of the form Me/MeOx are produced, for Me=Zn and Fe (see supplementary information Figure S4). However, when the particles are produced simultaneously with a rotating substrate holder, a completely different morphology of the particles is obtained, frequently presenting a flower-like morphology, as shown in Figure 1 (see supplementary information Figure S5). Phase-

contrast images (HR-TEM) in Figure 1b reveal different phases in the interior and exterior of the NPs. The inner part of the particles is formed by a monocrystalline phase, whose digital diffraction pattern may be attributed to a Fe phase (Figure 1c). The outer region of the particles corresponds to a polycrystalline material, with inter-planar distances to those of a Zn/ZnO. However, the unambiguous identification of the phases is hindered in the phase-contrast images and thus, a chemical characterization was carried out by EDS and EELS.

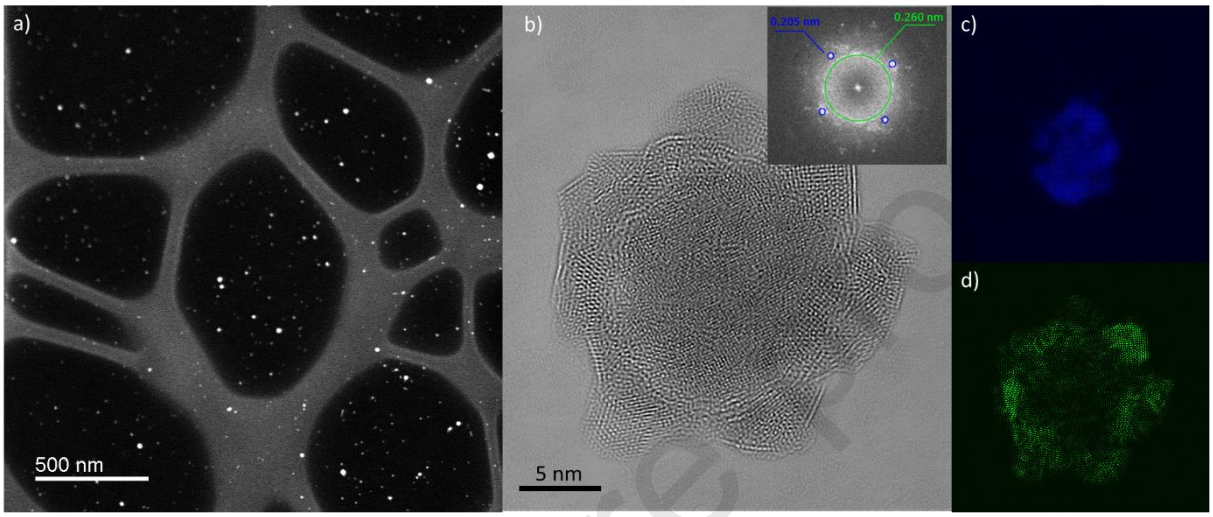

Figure 1. a) HAADF-STEM low magnification image of hybrid Zn-Fe nanoparticle deposited on ultra-thin carbon, b) phase-contrast image of a single particle. The inset corresponds to the FFT of the image, c) IFFT based on the FFT spots highlighted by the blue circles, c) IFFT based on the FFT highlighted in green.

The small and large NPs in Figure 1a have the same structure and are distributed on different zones of the surface, as shown in Figure S5. Moreover, figures 2a and 2b show the spectrum images from a single particle characterized by STEM-EDS and STEM-EELS. The results confirm the distribution of Zn and Fe from HR-TEM images, where the core is composed of Fe, surrounded by Zn NPs, forming flower-like nanoparticles. EELS spectra (Figure 2c) revealed a pure Fe phase in the core, and the existence of some Fe in the petals of the particles, forming a Zn(F)eO phase, which is also confirmed by EDS. It is worth noticing that the Fe core does not show an oxygen peak in the spectrum, which suggests that the major elements oxidized are located in the exterior of the particles. This is attributed to the galvanic protection that Zn offers to Fe. This oxidation control suggests that by adjusting the amount of Zn and Fe in the heterostructures, the oxidation of the particles can be tuned, allowing the use of these systems in applications such as oxygen scavenging and antibacterial properties.

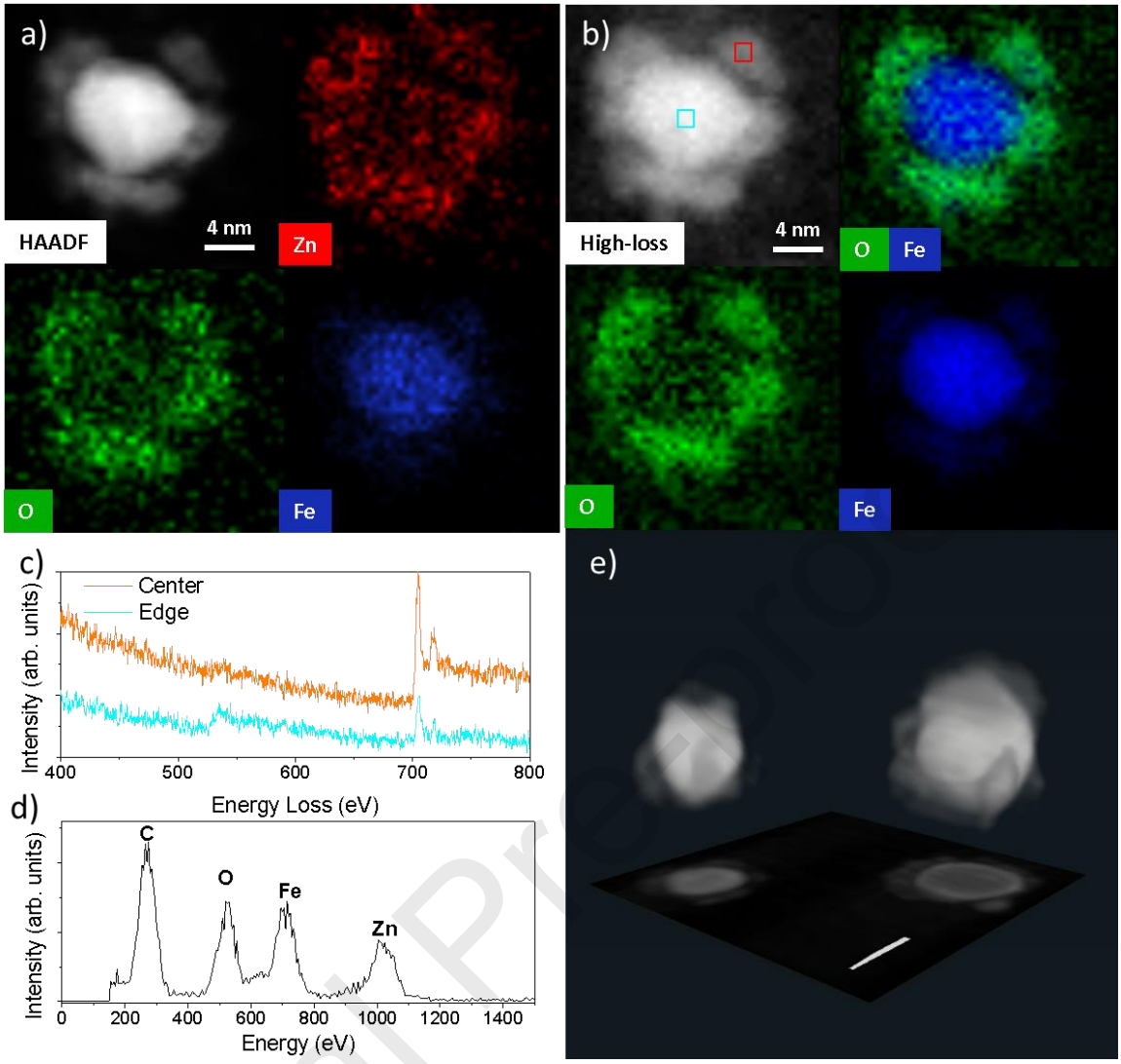

Figure 2. a) HAADF-STEM and EDS spectrum images for a bimetallic Zn-Fe NP, b) EELS spectrum images of the same NPs in a). c) EELS spectra from the core and edge of the blue and orange squares in b), respectively. d) EDS spectra of the particle shown in a), and e) reconstructed ZnFe NP using HAADF-STEM tomography.

2D projection from the (S)TEM does not allow us to determine the extent to which Zn covers the Fe core, and thus, to guarantee that such particles are not completely wrapping the Fe core, tomography studies were carried out. Figure 2e displays the particles after the 3D tomography reconstruction as well as their projection; clearly, the particles are formed by a core spherical particle decorated with smaller particles that shape the petals of the flower-like morphology. Such petals exist not only at the surface-plane of the substrate but also on the top of the particles, indicating a strong redistribution of the Zn nanoparticles.

Molecular dynamics simulations (MD) reveals the main mechanisms responsible for the restructuring of the NPs on the surface. Initially, the simulation shows that the clusters are freely moving on the surface, due to the low substrate-cluster interaction energy. After the impact, the iron NPs kinetic energy is partly degraded into heat, as can be seen by the NPs heating reported in Figure 3c, and also transferred to the substrate. Due to the large size of the substrate compared to the NPs, the temperature variation is negligible, and most of the energy is converted into mechanical energy, triggering substrate elastic modes. As a consequence Cu clusters are accelerated by NP impact in a way that is proportional to the incoming NPs energy, as depicted by their mean square displacement (MSD) in Figure 3d. This increased mobility means that all those phenomena related to surface diffusion, such as coalescence, are accelerated.

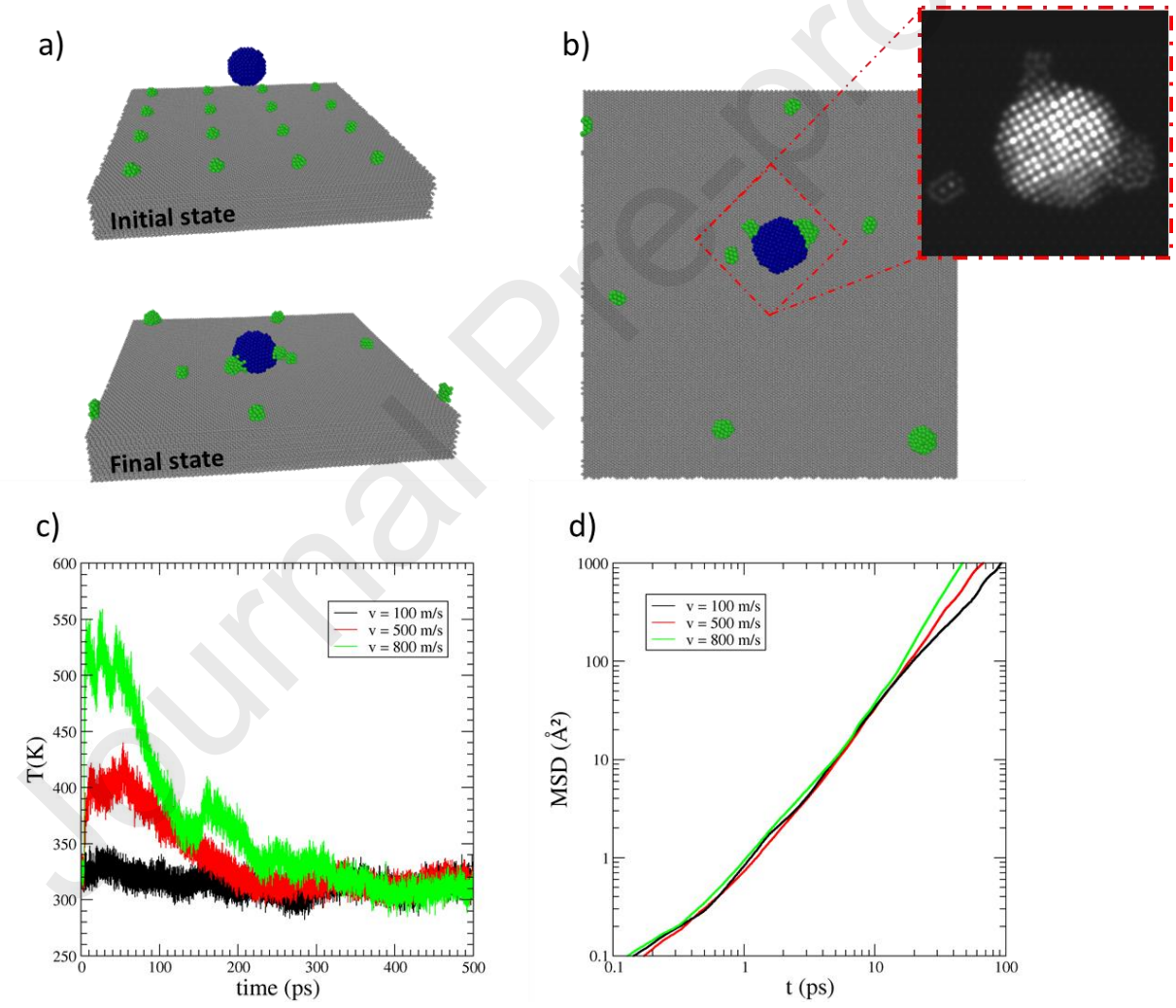

Figure 3. a) Simulated system before the equilibration of copper clusters and after 1 ns (Fe=blue, Cu=green and C=grey), b) top view of the simulated system after 1 ns; the inset in the image represents the STEM multislice computer-simulated images c) Temperature of the Fe NPs during impact and d) the mean square displacement of copper clusters on the substrate.

Another significant phenomenon, observed for large impact velocities, is the re-sputtering of Cu clusters from the surface due to the small adhesion energy of the Cu clusters (supplementary information). At all impact energies considered, the attachment of Cu clusters to the Fe NPs was observed. When re-sputtering occurs, the clusters can also attach on top of the Fe-NPs, and not only in correspondence of the substrate/surface contact.

We could deduce that the decoration of Fe-NPs Zn cluster occurs because the impact promotes the mobility of their on the surface, hence accelerating the coalescence of Fe and Zn NPs. Moreover, the fact that Zn is also observed on the top can be explained by impact-driven re-sputtering and subsequent adhesion of Zn clusters over the Fe NP.

Based on the MD simulation results, HAADF-STEM images simulation were carried out [9](Figure 3b inset). The images reveal a more intense core when compared to surrounding particles, which for HAADF images signify heavier elements or thicker regions. In this particular case, it is known that Zn, Fe and Cu would have very similar contrast due to the proximity in the atomic number, therefore the changes are mainly due to the size of the particles. Thus, the smaller size of the Zn clusters explains their different contrast in the STEM images, which, together with the tomography results, confirm the existence of smaller particles decorating the core.

Conclusion

Zn and Fe NPs were deposited simultaneously using a hybrid system based on a conventional magnetron sputtering and a cluster source. Phase-contrast images (HR-TEM) exhibited two different phases in the interior and exterior of the particles. The inner part is formed by a monocrystalline phase attributed to the Fe phase, while the exterior region of the particles corresponds to a polycrystalline of the Zn/ZnO. Besides, MD simulation demonstrated that the observed coverage of the Fe NPs occurs after the aggregation with Zn NPs, promoting Zn NPs diffusivity on the surface, hence accelerating the coalescence of Fe and Zn NPs. The samples properties that have been studied in the present investigation can be used in a wide range of including oxygen scavenging, antibacterial devices and bio-imaging technologies.

Acknowledgment

The authors thank the financial support by the Portuguese Foundation for Science and Technology (FCT) in the framework of the Strategic Funding UIDB/04650/2020 and by project NANOXYPACK co-financed via FEDER (PT2020) POCI-01-0145-FEDER-030789.

References

[1]Loza, K., Heggen,M. & Epple, M. Synthesis, Structure, Properties, and Applications of Bimetallic Nanoparticles of Noble Metals. *Adv. Funct. Mater.* **30**, (2020).

[2]Medina-Cruz, D. *et al.* Bimetallic nanoparticles for biomedical applications: A review. *Racing Surf.* 397–434 (2020).

[3]Basavegowda, N., Mandal, T. K. & Baek, K. H. Bimetallic and Trimetallic Nanoparticles for Active Food Packaging Applications: A Review. *Food Bioprocess Technol.* **13**, 30–44 (2020).

[4]Jamkhande, P. G.,Ghule, N. W., Bamer, A. H. & Kalaskar, M. G. Metal nanoparticles synthesis: An overview on methods of preparation, advantages and disadvantages, and applications. *J. Drug Deliv. Sci. Technol.* **53**, 101174 (2019).

[5]Calderon, S. V.,Gomes, B., Ferreira, P. J. & Carvalho, S. Zinc nanostructures for oxygen scavenging. *Nanoscale* **9**, 5254–5262 (2017).

[6]Zhao, J. *et al.* Formation Mechanism of Fe Nanocubes by Magnetron Sputtering Inert Gas Condensation. *ACS Nano* **10**, 4684–4694 (2016).

[7]Vernieres, J. *et al.* Gas Phase Synthesis of Multifunctional Fe-Based Nanocubes. *Adv. Funct. Mater.* **27**, (2017).

[8]*S*. Plimpton, Fast parallel algorithms for short-range molecular dynamics, Journal of Computational Physics 117 (1) (1995) 1 – 19. https://doi.org/10.1006/jcph.1995.1039

[9]*J. Barthel,Dr. Probe: A software for high-resolution STEM image simulation. Ultramicroscopy 193 (2018)*

CRediT author statement

H. Lamsaf: Production of the materials, Editing and Reviewing.

V. Lenzi: Molecular dynamic simulations, Writing, Editing and Reviewing.

L. Marques: Supervision of the molecular dynamics simulations, Methodology.

L. Rebouta: Supervision of the production of the materials.

S. Carvalho, L. F. Ballesteros, M. A. Cerqueira, J. A. Teixeira, L. Pastrana: Editing, Reviewing, Funding acquisition.

S. Calderon V: Supervision of the materials production, Conceptualization, Methodology, Writing-Reviewing, Editing and Funding acquisition.

Highlights

- Hybrid sputtering/ gas agglomeration system produces flower-like Zn-Fe NPs.
- Fast, simple and reliable method to produce bimetallic nanoparticles.
- Molecular dynamics shows the growth mechanisms of the particles.
- Galvanic couple between Zn –Fe protects Fe from oxidation.

Declaration of interests

☒ The authors declare that they have no known competing financial interests or personal relationships that could have appeared to influence the work reported in this paper.

☐The authors declare the following financial interests/personal relationships which may be considered as potential competing interests:

Supplementary Information

Zn-Fe Flower-Like Nanoparticles Growth by Gas Condensation

H. Lamsaf [1,2], V. Lenzi [1], L. Marques [1], L. Rebouta [1], S. Carvalho [4], L. F. Ballesteros [1,3], M. A. Cerqueira [2], J. A. Teixeira [3], L. Pastrana [2], S. Calderon V [1,2] *.

[1] CF-UM-UP, Centre of Physics of Minho and Porto Universities, Campus of Azurém, 4800-058 Guimarães, Portugal

[2] INL - International Iberian Nanotechnology Laboratory, Av. Mestre José Veiga s/n, 4715-330 Braga, Portugal

[3] CEB – Centre of Biological Engineering, University of Minho, Campus de Gualtar, 4710-057 Braga, Portugal

[4] SEG-CEMMPRE, Mechanical Engineering Department, University of Coimbra, 3030-788 Coimbra, Portugal

Materials production

All nanoparticles (NPs) of Zn, Fe, or Zn-Fe were produced using a hybrid sputtering equipped with a cluster gun. The scheme presented in **Figure S1** shows the setup apparatus where all samples were produced, which is composed of two principal parts: (i) the main chamber with an internal diameter of 40 cm connected with a vacuum system, where the Zinc target (99.9% of purity, Ø = 50.8 mm, and thickness 4.5 mm) was located at 6 cm from the substrate holder, and (ii) a DC cluster beams source linked with water cooling system, with a Fe target (99,95% of purity, Ø = 6.9 cm and thickness 3 mm, The cluster gun has two nozzles with 2.5 mm and 4 mm of diameters, respectively. The distance between the Fe magnetron and the cluster gun inner aperture was 8 cm and the rotating substrate holder was located 10 cm away from the outer aperture of the cluster gun. The nozzles created a differential pressure, which permitted the passing of the cluster beams toward the main chamber.

The main chamber and the cluster beam were evacuated with an initial pressure of 1 x10^{-4} Pa and 0.02 Pa, then set up to a working pressure of 0.8 Pa to 70 Pa, respectively, with the presence of Argon as a sputtering gas introduced in the cluster gun chamber (Φ Ar = 50 sccm). The substrates were in static mode for samples Zn and Fe in order to optimize parameters to produce NPs from each target, whereas were rotated with a speed of 2 rpm for the hybrid nanoparticles.

All samples were deposited onto substrates of Si-wafers, TEM Cu-grids with ultra-thin carbon layers (400 mesh) and glass. The Si and glass substrates were cleaned by distilled water, acetone, and ethanol for 10 min sequentially in order to remove impurities on the surface. Table S1 presents the parameter details used to produce Zn and/or Fe NPs.

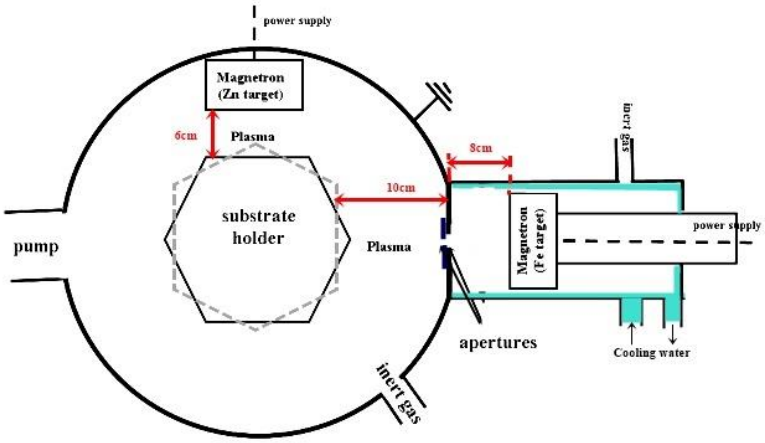

Figure S1. Schematic of the cluster chamber.

Table S1. Process parameters.

Process mode		J_{Zn} (mA/cm^2)	J_{Fe} (mA/cm^2)	Zn+Fe layer time (min)	Rate(nm/mn)
static	**Zn**	2.96	--	8 *	70
static	**Fe**	--	2.67	15 **	80
rotated	**ZnFe**	2.96	2.7	1	--

(*) only Zn (**) only Fe

Materials Characterization

Scanning transmission electron microscopy (STEM – EDS)

High angle annular dark-field (HAADF) STEM and phase-contrast images were acquired on a double corrected FEI Titan Themis operated at 200 keV. HAADF-STEM images were recorded using a convergence angle of 21 mrad with a pixel dwell time set at 10µs. A camera length of 115 mm was selected, which allows the HAADF detector to collect electrons between 50 and 200 mrad.

Energy-dispersive X-ray spectroscopy mappings (EDS-mapping) in transmission mode was performed in double corrected FEI Titan Themis operated at 200 keV equipped with a Super-X EDX detector. Iterative maps of 512 x 512 pixels were recorded with a dwell time per pixel of 10 µs at 200 keV to determine the elemental distribution. The current of the electron beam was maintained as constant as possible in all the samples between 200 and 250 pA, and the maps were acquired for 15 min.

Electron Energy Loss Spectroscopy (EELS)

Electron Energy Loss Spectroscopy (EELS) was performed on a double corrected FEI Titan Themis, operated at 200 keV, equipped with a dual-EELS Enfinum ER spectrometer. The STEM-EELS spectrum images (SI) were acquired with a spectrometer channel resolution of 0.1 eV with a 5 mm aperture, so that a resolution between 1 to 1.2 eV is achieved. The Fe $L_{3,2}$-edges were collected using $5x10^{-2}$ s per pixel, while the zero-loss peak was simultaneously collected for $5x10^{-5}$ s per pixel. The beam convergence angle was set at 21 mrad, and the camera length was adjusted to 29.5 mm to position the majority of the electrons in the entrance of the spectrometer.

Tomography

A Fischione single tilt tomography holder was used to acquire HAADF-STEM images at 80 kV, in an angular increment of 5° and a tilt range of ±70°. Manual alignment was used, due to the size of the particles, to center the specimen at each tilt angle. Spatial image alignment was performed using cross-correlation of HAADF images in FEI's Inspect3D software package. Tilt axis alignment was also undertaken in Inspect3D followed by reconstruction with 100 iterations.

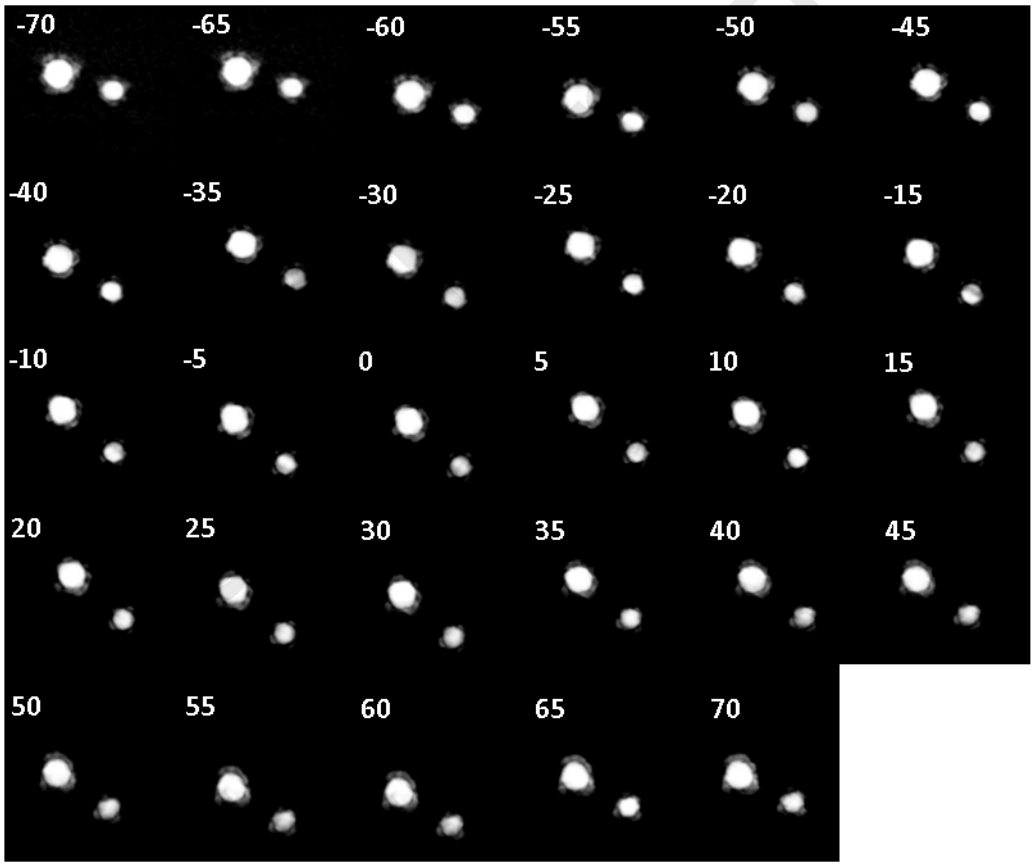

Figure S2. HAADF images acquired at an angular increment of 5° and a tilt range of ±70° of two ZnFe bimetallic nanoparticles.

Molecular dynamics simulations

Molecular modelling and simulations are used to investigate molecular phenomena that are difficult to observe experimentally. If, on one side, the adopted theoretical models rely on various simplifying assumptions that makes the simulations actually feasible. On the other side, the underlying physics of the studied phenomenon is fully known, hence providing precious insights. Thus, to model the experimental system, a substrate of 9 graphite layers was considered, lying in the xy plane, with a depth of 3 nm and a lateral size of 20 nm in each direction. The surface was decorated with 16 copper clusters, containing 28 atoms each. An iron nanoparticle with a diameter of 2.8 nm was created above the surface. Copper was chosen in lieu of Zn because of the lack of a suitable molecular dynamics force-field for the iron-zinc pair. However, because of their similar atomic masses, Cu clusters should represent closely the behaviour of Zn ones. The Cu-Fe interatomic interaction the MEAM force field was adopted [1] [2][. In particular, the parametrizations of Jelinek [3] was used for iron and copper, while the parametrization of Liyanage [4] was used for carbon. Lennard-Jones potentials were added between atoms of adjacent graphite sheets to reproduce the correct interlayer spacing. The interaction between metal atoms and graphite was modelled using LJ potentials as well, chosen to reproduce the atomic adsorption energies for Fe and Zn on graphene. All simulations were performed using LAMMPS.

The nanoparticle impact implies a large transfer of momentum causing the appearance of large forces within the simulation, which might render the MD integration unstable if a too large time-step is chosen. For this reason, time step of 0.1 fs was adopted, which ensures the correct description of particle motion and total energy conservation. All simulations were performed under NVE conditions, except for a 2 Å thick region at the edges of the substrate, for which NVT conditions were employed, with the temperature being fixed at 300 K and using a coupling constant of 10 fs. The center of mass of the NVT region was kept fixed. In this way, the mechanical and thermal coupling of the substrate with the support is reproduced, providing a way for energy dissipation.

The nanoparticle and the graphite substrate were heated up at 300 K and equilibrated under NVT conditions. Next, the cluster was deposited on the substrate, such as shown in **Figure S3**. The substrate acts as a heat reservoir for the clusters so that a 100 ps run was sufficient to heat them to the substrate temperature. At this point, a net negative speed along the z-axis was set to all atoms of the iron NP, in order to trigger the impact, which was followed for 1 ns. Speeds of 100, 500 and 800 m/s were considered.

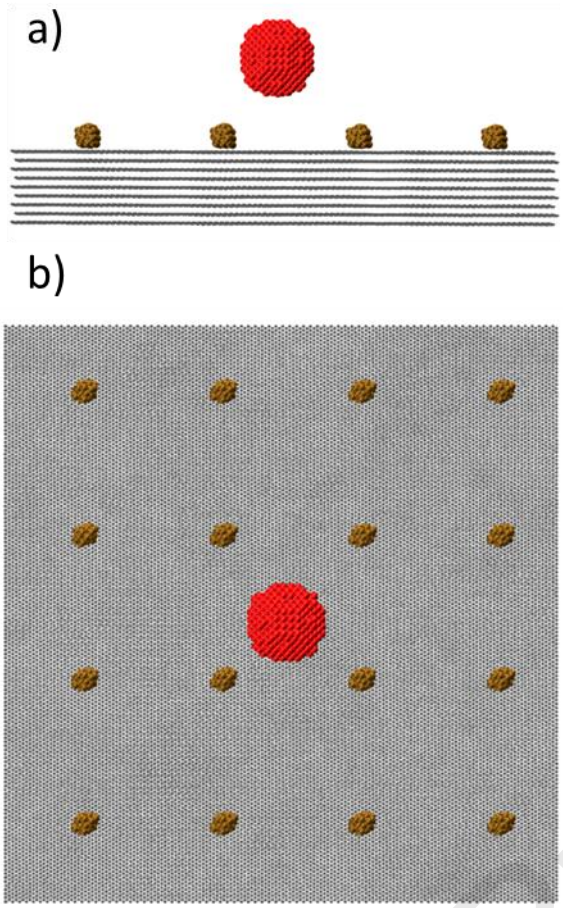

Figure S3. a) side and b) top view of the simulated system before the equilibration of Cu clusters. Fe is depicted by red spheres, Cu by ochre ones and C atoms by grey dots.

STEM multislice images simulation

Simulation of HAADF images was carried out using Dr. Probe V1.9 software package, [5] using the final frame of the MD, with the beam perpendicular to the substrate surface. Frozen-lattice configuration was used and the simulation was carried out reproducing the experimental conditions at 200 kV and 21 mrad aperture.

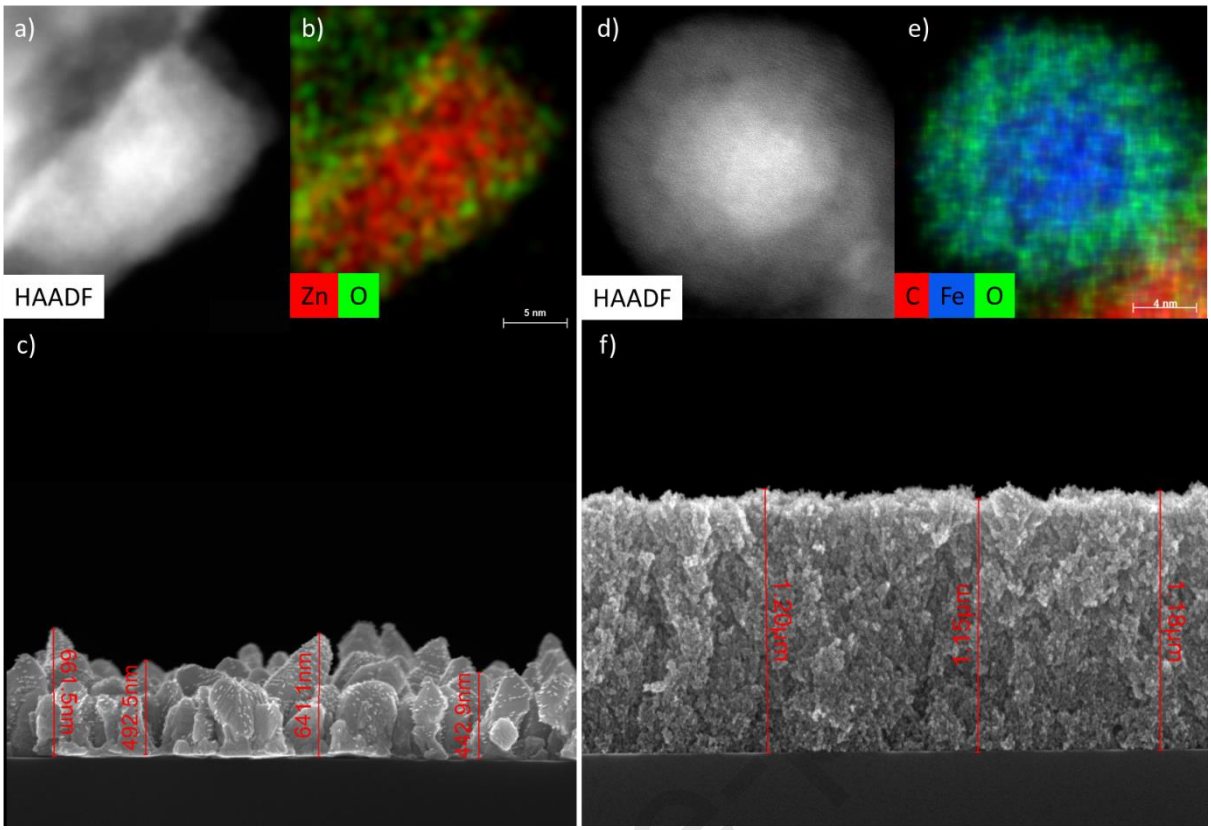

Figure S4. a) HAADF-STEM and b) EDS spectrum images acquired for particles Zn/ZnO particles deposited using conventional magnetron sputtering, c) thick coating of Zn using conventional magnetron sputtering, d) HAADF-STEM and e) EDS spectrum images acquired for particles Fe/FeO_x particles deposited using cluster gun, and f) thick coating of Fe using cluster gun.

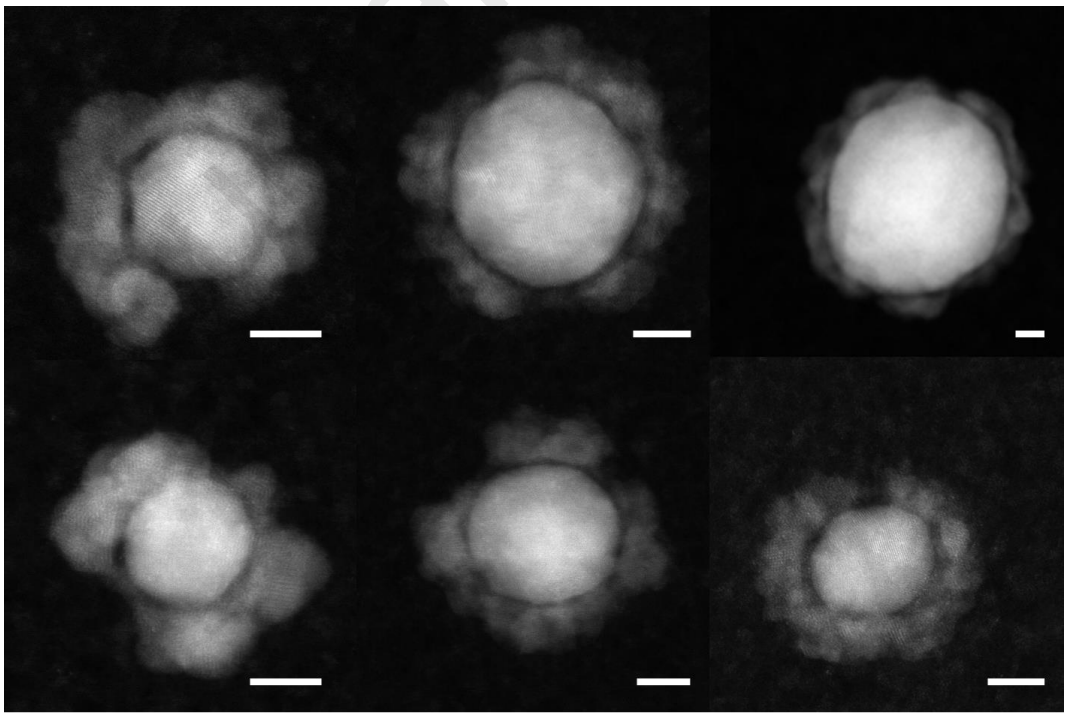

Figure S5. HAADF – STEM images of a set of flower-like nanoparticles. Scale bar represents 5 nm.

[1] M. I. Baskes, Modified embedded-atom potentials for cubic materials and impurities, Phys. Rev. B, 46:5 (1992) 2727-2742. https://doi.org/10.1103/PhysRevB.46.2727

[2] B. J. Lee, M. I. Baskes, H. Kim and Y. Koo Cho, Second nearest-neighbor modified embedded atom method potentials for bcc transition metals, Phys. Rev. B, 64:18 (2001) 184102. https://doi.org/10.1103/PhysRevB.64.184102

[3]B. Jelinek, S. Groh, M. F. Horstemeyer, J. Houze, S. G. Kim, G. J. Wagner, A. Moitra, and M. I. Baskes, Modified embedded atom method potential for Al, Si, Mg, Cu, and Fe alloys, Phys Rev B 85 (2012) 245102. https://doi.org/10.1103/PhysRevB.85.245102

[4]L. S. I. Liyanage, S. G. Kim, J. Houze, S. Kim, M. A. Tschopp, M. I. Baskes and M. F. Horstemeyer, Structural, elastic, and thermal properties of cementite (Fe 3 C) calculated using a modified embedded atom method, Phys. Rev. B 89 (2014) 094102. https://doi.org/10.1103/PhysRevB.89.094102.

[5] *J. Barthel, Dr. Probe: A software for high-resolution STEM image simulation. Ultramicroscopy 193 (2018)*